WATER RESOURCES RESEARCH, VOL. 36, NO. 11, PAGES 3311–3324, NOVEMBER 2000

Saturated hydraulic conductivity and soil water retention properties across a soil-slope transition

Binayak P. Mohanty
U.S. Salinity Laboratory, Riverside, California

Zak Mousli
University of California Bay Area Research and Extension Center, Santa Clara, California

Abstract. The hydraulic properties of soil and their spatial structures are important for understanding soil moisture dynamics, land surface and subsurface hydrology, and contaminant transport. We investigated whether landscape features, including relative position on a slope, contribute to the variability of soil hydraulic properties in a complex terrain of a glacial till material. Using 396 undisturbed soil cores collected along two orthogonal transects, we measured saturated hydraulic conductivity (K_{sat}) and soil water retention functions at two (15 and 30 cm) depths across a glacial till landscape in central Iowa that encompassed two soil types (Nicollet loam with 1–3% slope on the hilltop position and Clarion loam with 2–5% slope on the shoulder position). The van Genuchten-Mualem model was fitted to the experimental data using the RETC optimization computer code. At the 15 cm depth a statistical comparison indicated significant differences in K_{sat}, saturated water content (θ_s), water content at permanent wilting point ($\theta_{15,000}$), and van Genuchten fitting parameters (α and n) between soil types and landscape positions. At the 30 cm depth, θ_s, $\theta_{15,000}$, and residual water content (θ_r) were found to be significantly different across the soil-slope transition. Available water content ($\theta_{333-15,000}$) did not show any significant difference across the soil-slope transition for either depth. No clear directional trend was observed, with some exceptions for K_{sat}, θ_s, and α on specific transect limbs and depths. Drifts in the soil hydraulic parameters due to soil-slope transition were removed using a mean-polishing approach. Geostatistical analyses of these parameters showed several important characteristics including the following: (1) The spatial correlation lengths and semivariogram patterns of the independently measured (or estimated) $\log_e K_{sat}$ and θ_s at 30-cm depth matched extremely well; (2) better spatial structures with large correlation lengths were observed for (macro and micro) porosity-related $\log_e K_{sat}$, θ_s, and $\log_e \alpha$ than for texture-related $\log_e \theta_{333-15,000}$, $\log_e \theta_{15,000}$, θ_r, and $\log_e n$ at 30-cm depth; and (3) a higher nugget effect at 15-cm depth was evident for most soil hydraulic parameters, indicating tillage and other surface disturbances. These novel findings may prove to be critical for modeling and interpreting field-scale or larger-scale soil moisture dynamics, surface and subsurface flow, and solute transport.

1. Introduction

Soil, topography, vegetation, and precipitation interactively govern hydrology and contaminant transport in the land-surface and near-surface environment. Furthermore, characteristic features of these factors are interlinked by landscape and plant-habitat evolution. Understanding the interrelationship between soil variability and landscape features is a key to understanding the soil hydrologic environment. For example, soil hydraulic properties may vary along a slope, resulting in variability in surface soil moisture and subsurface drainage, as well as in nonpoint source contaminant loading. Measurements of hydraulic properties cutting across different soil types, slopes, vegetation, and precipitation fields are scarce. From the land surface hydrologic perspective, *Loague and Gander* [1990], *Elsenbeer et al.* [1992], and *Famiglietti et al.* [1998] are among the few who have reported the variability of selected soil properties along slopes in surface soil moisture studies. *Loague and Gander* [1990] and *Sharma et al.* [1980] reported steady state infiltration rates collected in a rangeland catchment that cut across three different soil types and a gentle slope of 3%. *Elsenbeer et al.* [1992] did a detailed survey of saturated hydraulic conductivity (K_{sat}) on different slope units with a maximum side slope of 70% in a tropical rain forest catchment. *Famiglietti et al.* [1998] measured particle size and porosity across a 5% slope to study the combined influence of soil properties and topographic features on the spatial distribution of surface soil moisture. P. J. Shouse et al. (U.S. Salinity Laboratory, unpublished report, 2000) conducted extensive soil property measurement cutting across different soil, slope, vegetation, and climatic conditions during the Southern Great Plains 1997 (SGP97) hydrology experiment in Oklahoma.

From an environmental perspective, studies on the variability of soil properties are relatively abundant. *Sauer et al.* [1998] characterized the properties of soil at different landscape po-

Paper number 2000WR900216.
0043-1397/00/2000WR900216$09.00

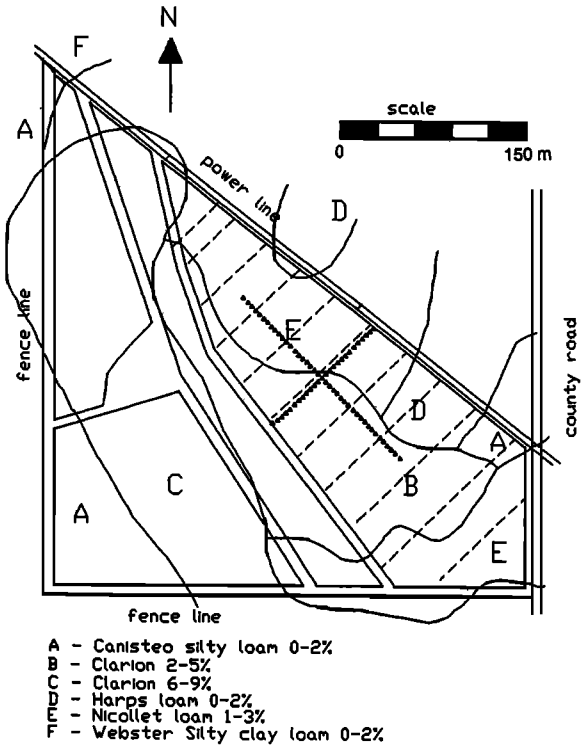

Figure 1. Soil-slope map of the experimental field with two orthogonal sampling transects (NE-SW and NW-SE).

sitions in the Ozark highlands to study the transport of animal manures. They measured soil texture, saturated hydraulic conductivity, bulk density, and chemical properties of soil. *Hussain et al.* [1998] demonstrated the long-term effects of tillage on physical properties influencing soil erosion on a sloping and eroded soil in southern Illinois. *Mohanty et al.* [1994], *Logsdon and Jaynes* [1996], and *Azevedo et al.* [1998] reported near-saturated hydraulic conductivities for four different soil water pressure heads and associated the observed spatial variability with differences in soil tillage practices, growing seasons, and rainfall events. Most studies have focused on addressing (near saturated) preferential flow-transport processes; only a few studies have reported the spatial variability of soil hydraulic properties for the complete soil water tension range (e.g., up to the permanent wilting point, 15,000 cm of H_2O). For example, *Mallants et al.* [1996] studied the spatial correlation structures of the complete soil water retention range (0–15,000 cm of H_2O) in Bekkevoort, Belgium, for flow transport in a multilayered soil profile. Their study, however, was limited to a small plot with uniform soil and topography. Some of the other better known spatial variability studies of hydraulic properties were conducted by *Russo and Bresler* [1981] in Bet Dagan, Israel, *Gajem et al.* [1981] in Marana, Arizona, and *Unlu et al.* [1990] in Davis, California. As with *Mallants et al.* [1996], these studies were limited to uniform soil type and topography.

In general, soils derived from glacial deposits are considered complex and spatially variable. Researchers have concluded that the influence of genesis on various properties of till and diamicton materials occurs primarily as a result of gross differences in depositional environment and that supraglacial deposits are highly variable compared with basal till. Furthermore, they determined that the postdepositional changes in glacial deposits can produce a complex set of effects on the behavior of the till soil. In this paper, we will study the variability of K_{sat} and soil water retention properties ($\theta(h)$) across a soil-slope transition in a glacial till material in Iowa. The objectives of this study include (1) measurement of K_{sat} and θ (h equals 10 cm to 15,000 cm H_2O) at a large number of spatial locations for two (15 and 30 cm) depths, (2) optimization of *van Genuchten* [1980] soil water retention parameters (θ_s, θ_r, α, and n), (3) statistical comparison of the measured (K_{sat}, water content at permanent wilting point $\theta_{15,000}$, and available water content or water-holding capacity $\theta_{333-15,000}$ as defined by *Cassel and Nielsen* [1986]) or estimated (θ_s, θ_r, α, and n) hydraulic parameters across an existing soil-slope transition, and (4) geostatistical (structural) analysis and modeling of the soil hydraulic parameters across the experimental field.

2. Materials and Methods

The experimental site in this study was a 115 m × 183 m field at the Agronomy and Agricultural Engineering farm near Boone in central Iowa. The general landscape of this part of the country is rolling, with soils developed from a glacial till deposition (Des Moines lobe) of Wisconsin age. The two major soil types in this field are the Nicollet loam (fine-loamy, mixed, mesic Aquic Hapludoll) and the Clarion loam (fine-loamy, mixed mesic Typic Hapludoll), both derived from glacial till, with a transition line somewhat along NW-SE direction (Figure 1 [*U.S. Department of Agriculture*, 1984]. The soils are part of the Nicollet-Clarion-Webster soil association, where Nicollet lies on the hilltop, Clarion lies on the slope, and Webster lies in the valley positions. The slope in the field ranged between 0 and 5% depending on depositional pattern. Slope varied between 2 and 5% for Clarion loam (B) and between 1 and 3% for Nicollet loam (E). This field was chosen to complement other hydrologic and water quality studies at the site [*Mohanty et al.*, 1991; *Mohanty and Kanwar*, 1994; *Mohanty et al.*, 1998]. It had been under no-tillage management for 6 years prior to our experiment in 1989.

2.1. Hydraulic Property Measurement Methods

During the corn planting season we collected undisturbed soil cores (76-mm diameter and 76-mm length) along two orthogonal transects at 66 sampling sites (4.6-m intervals) and two depths (15 cm and 30 cm). The transects were oriented in the NW-SE and NE-SW directions and intersected near the boundary of the Nicollet and Clarion series, with the NW and NE limbs of the transects located in the Nicollet loam and the SW and SE limbs located in the Clarion loam (Figure 1). Three soil cores were taken at each site and depth (within a 0.5-m neighborhood) for a total of 396 (3 × 2 × 66) cores. All soil cores were collected using an Uhland sampler with the core center matching the sampling depth and were taken from crop rows to avoid soil compacted by wheel traffic, which has a significantly lower saturated hydraulic conductivity because of reduced total porosity and macroporosity [*Mohanty et al.*, 1994]. After discarding a few bad samples, 185 samples for the 15-cm depth and 188 samples for the 30-cm depth were analyzed for saturated hydraulic conductivity (K_{sat}) using a constant head permeameter in the laboratory [*Klute*, 1986]. In the interests of time and labor a subset of 134 samples (Figure 2) was randomly chosen for unsaturated hydraulic conductivity and soil water retention measurements between 10 and 15,000 cm of H_2O using Tempe cells and pressure plate apparatuses. Measurements were made in eight to 10 tension steps for five

different batches (e.g., 15, 35, 49, 129, 320, 1000, 5000, and 15,000 cm of H_2O for batch 2). We limited our measurements to a lowest tension of 10 cm of H_2O because the soil water retention measurements near saturation were not precise. Soil water retention measurements up to a tension of 500 cm of H_2O were made on the entire 76-mm-long soil samples using the multistep outflow approach in Tempe cells, followed by pressure plate measurements on 10-mm-long subsamples at higher tensions [*Klute*, 1986]. In the relatively wet range (up to 100 cm of H_2O) an average of 24 hours was needed for the soil cores to equilibrate to the imposed soil water tension. For the intermediate to dry range, equilibration time for the soil cores increased to several days or weeks. All laboratory measurements were accomplished within a period of 2 years at the hydraulics and soil physics laboratories of Iowa State University. In this study, we focus on the effect of soil type and landscape position on saturated hydraulic conductivity and soil water retention data. An analysis of the soil water retention and unsaturated conductivity data sets will be presented in the future.

2.2. Soil Water Retention Function

Assuming a unimodal pore size distribution, the *van Genuchten* [1980] soil water retention function with Mualem pore size distribution model was assumed to describe our data. The expressions of *van Genuchten* [1980] are

$$\theta(h) = \theta_r + \frac{\theta_s - \theta_r}{[1 + |\alpha h|^n]^m} \qquad h < 0, \tag{1}$$

$$\theta(h) = \theta_s \qquad h \geq 0, \tag{2}$$

where

$m = 1 - 1/n$ for $n > 1$;
h soil water pressure head $[L]$;
θ volumetric water content of soil $[L^3\ L^{-3}]$;
θ_r residual soil water content $[L^3\ L^{-3}]$;
θ_s saturated soil water content $[L^3\ L^{-3}]$;
α fitting parameter in the soil water retention function $[L^{-1}]$;
n fitting parameter in the soil water retention function [dimensionless].

The significance of these model parameters, including the advantages and limitations of the Mualem constraint ($m = 1 - 1/n$), were discussed in detail by *van Genuchten et al.* [1991]. For example, allowing m and n to vary independently leads to a complicated form of the predictive equation for the unsaturated hydraulic conductivity. However, imposing the restriction $m = 1 - 1/n$ forces the shape and curvature of the retention curve near saturation to have a unique relation with the shape and slope of the curve in the dry range when $\alpha h \gg 1$. While the restriction $m = 1 - 1/n$ limits the flexibility of (1), its effect on the hydraulic conductivity curve is not clear. More analysis and discussion of these and related topics are given by *Yates et al.* [1992]. We will test some of their hypotheses using our soil water retention and unsaturated hydraulic conductivity data during the future comparative analysis.

2.3. Parameter Estimation

We analyzed the steady state soil water retention data, $\theta(h)$, using the RETC optimization software [*van Genuchten et al.*, 1991]. Our soil water retention model contained four independent parameters, i.e., θ_r, θ_s, α, and n. The model parameters were represented by the parameter vector $\mathbf{b} = (\theta_r, \theta_s, \alpha, n)$. The RETC optimization model can fit any one, several, or all of these parameters simultaneously to observed data. With our wide range (10 to 15,000 cm of H_2O) of measurements we opted for the simultaneous fit of all four parameters to avoid any judgmental error in fixing θ_r or θ_s without exact measurements. RETC uses a nonlinear least squares optimization approach based on *Marquardt*'s [1963] maximum neighborhood method to estimate the unknown model parameters from observed retention data. The objective function was given by

$$O(\mathbf{b}) = \sum_{i=1}^{N} \{w_i[\theta_i - \theta_i^*(\mathbf{b})]\}^2, \tag{3}$$

where θ_i and θ_i^* are the observed and fitted water contents, respectively, and N is the number of retention data points. The weighting coefficients w_i in (3) may be used to assign more or less weight to a single data depending upon a priori information. We used equal (unity) weights (w_i) for all data points (i) assuming that all measurement steps have the same amount of uncertainty, reducing the problem to an ordinary least squares fitting problem.

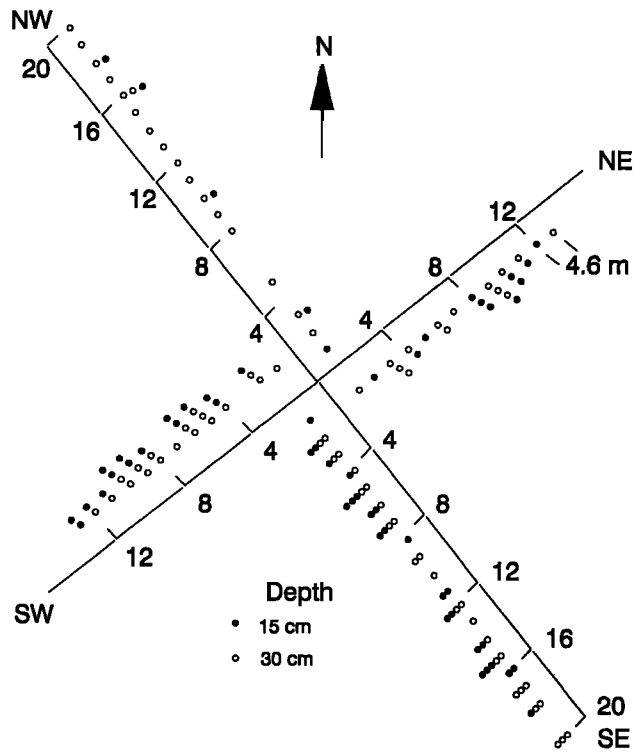

Figure 2. Location of selected soil cores along the transects used for the soil water retention measurements at the 15-cm and 30-cm depths.

2.4. Spatial Analysis

Geostatistics in conjunction with exploratory data analysis [*Tukey*, 1977] were used to study the spatial structure of the soil hydraulic parameters. On the basis of normality and stationarity assumptions, experimental variograms were the main tools used to explore the spatial structure of these parameters. Because these semivariograms can provide the basis for further geostatistical assessment and can generate spatial fields of soil

hydraulic properties, accurate analysis and pretreatment of data are needed before developing semivariograms. The intrinsic hypothesis [*Matheron*, 1963] makes the following stationarity assumptions for the regionalized variable $Z(x)$: (1) $E\{Z(x + h) - Z(x)\} = 0$ for any x and h (in other words, one expects $Z(x)$ to be constant for any x and h in Γ) and (2) $2\gamma(h) = E\{[Z(x + h) - Z(x)]^2\}$ for any x and h, where $\gamma(h)$ is a semivariogram estimator which states that variance of the difference in soil property depends only on the separating vector h. Following *Matheron* [1963], *Journel and Huijbregts* [1978] studied spatial variability using semivariograms and defined an average semivariogram $\gamma^*(h)$ in a specific direction

$$\gamma^*(|h|, \varphi) = \frac{1}{2N(|h|, \varphi)} \left\{ \sum_{i=1}^{N} Z(x_{i+|h|}) - Z(x_i) \right\}^2 \quad (4)$$

where $\gamma^*(|h|, \varphi)$ is a semivariogram estimator, φ implies direction, $|h|$ is the modulus of interval, N is the number of pairs of the regionalized variable having a specified separating vector, and $Z(x_i), \ldots, Z(x_n)$ are soil hydraulic parameter data taken at $x_i, \ldots, x_n$. *Journel and Huijbregts* [1978, pp. 175 and 262] reported that the semivariogram may be directionally dependent and that data can be checked for anisotropy by computing $\gamma^*(|h|, \varphi)$ for different φ. Note that for field data, the separation vector $(|h|, \varphi)$ would represent a range of values rather than a particular value. Before estimating isotropic and directional semivariograms, stationarity in the means and variances across the soil-slope transition was examined as a prerequisite. Exploratory schemes [*Tukey*, 1977; *Mohanty et al.*, 1991; *Cressie*, 1993; *Mohanty and Kanwar*, 1994] are simple yet powerful tools to overcome nonstationarity within the experimental data. Normal probability plots of raw and $\log_e$-transformed data were developed to examine the data distribution. Subsequently, a simple mean-polishing scheme was adopted to remove any associated drift in the normalized data sets across the soil-slope transition. Therefore the normalized data set is assumed to follow the relation

$$Z(x) = \mu(x) + \varepsilon(x), \quad (5)$$

where $Z(x)$ denotes the normal (raw or $\log_e$ transformed) regionalized variable at location (x), $\mu(x)$ is a measure of central tendency, that is, deterministic drift of the variable at location (x), and $\varepsilon(x)$ is the random component at location (x) normally distributed with zero mean, which satisfies the stationarity condition required for semivariogram estimation.

We evaluated the experimental semivariograms by fitting them to theoretical models. Various methods (jackknifing, nonlinear least squares techniques, and fitting by eye) are traditionally used to fit theoretical models to experimental semivariograms. Four isotropic models typically encountered in practice include linear, spherical, exponential, and Gaussian models, each of them defined in terms of nugget variance (C_0), sill (structural variance C plus nugget variance C_0), and correlation range parameters (A_0) as defined below. For the sake of completeness we briefly describe these theoretical models here. Detailed characteristics of these models can be found in standard geostatistics texts [e.g., *Journel and Huijbregts*, 1978]. The models are

Linear isotropic

$$\gamma(h) = C_0 + [h(C/A_0)], \quad (6)$$

Spherical isotropic

$$\gamma(h) = \begin{cases} C_0 + C[1.5(h/A_0) - 0.5(h/A_0)^3] & h \le A_0 \\ C_0 + C & h > A_0, \end{cases} \quad (7)$$

Exponential isotropic

$$\gamma(h) = C_0 + C[1 - \exp(-h/A_0)], \quad (8)$$

Gaussian isotropic

$$\gamma(h) = C_0 + C[1 - \exp(-h^2/A_0^2)]. \quad (9)$$

In addition to the isotropic models, geometrically anisotropic models are used for directional semivariograms, which presume different C and ranges for each direction examined but identical C_0. The correlation range (A_0) for the anisotropic (linear, spherical, exponential, or Gaussian) model is characterized by the range for the major axis Φ (A_1), the range for the minor axis $\Phi + \pi/2$ (A_2), the angle of maximum variation (Φ), and the angle between pairs (φ). It is defined as

$$A_0 = A_1^2[\cos^2(\varphi - \phi)] + A_2^2[\sin^2(\varphi - \phi)]. \quad (10)$$

For the linear model, A_0 is a range parameter (not range) and should not be compared directly with the A_0 of other models. For exponential and Gaussian models the range is usually assumed to be the point at which the model includes 95% of the sill $(C_0 + C)$; this can be estimated as $3A_0$ for the isotropic model or $3A_1$ $(3A_2)$ for the major (minor) axis in the anisotropic model. Therefore direct comparison of correlation ranges for different theoretical models should be made diligently. We used a geostatistical program (GS^+, Gamma Design Software, Plainwell, Michigan) for calculating experimental semivariograms and fitting them to different theoretical models using the nonlinear least squares techniques of *Marquardt* [1963].

3. Results and Discussion

3.1. Exploratory Analysis and Pretreatment of Data

Measured saturated hydraulic conductivities across the soil-slope transition (Nicollet loam with 1–3% slope on the hilltop and Clarion loam with 2–5% slope on the shoulder position) are presented in Figure 3. K_{sat} data are the average for three replicates at each grid location. This special treatment for K_{sat} was adopted to minimize the effect of any exceptionally high value due to the presence of any open-ended macropore in a sample. No clear directional trend in K_{sat} for the two soil-slope combinations is evident in these plots except on the NW-SE transect at 15-cm depth. Mean comparison (at 5% probability level) of K_{sat} between Nicollet loam and Clarion loam, however, showed a significant amount of drift (i.e., shift in the mean estimates) across the soil-slope transition for the 15-cm depth (Table 1). Furthermore, statistical comparison between the two depths indicated significantly higher K_{sat} at 30-cm depth than at 15-cm depth for both soil-slope combinations. The higher K_{sat} value is consistent with our visual observation of a large number of continuous (open-ended) macropores (root channels and earthworm burrows) in the soil cores collected at 30-cm depth. While small sample volume (76-mm length and 76-mm diameter) is an important factor contributing to the continuity of the macropores at 30-cm depth, tillage, slaking due to precipitation, and other surface disturbances limited the continuity of macropores at 15-cm depth. Furthermore, in a parallel study at the field site, *Singh et al.* [1991] found that the macropores (worm holes and root channels)

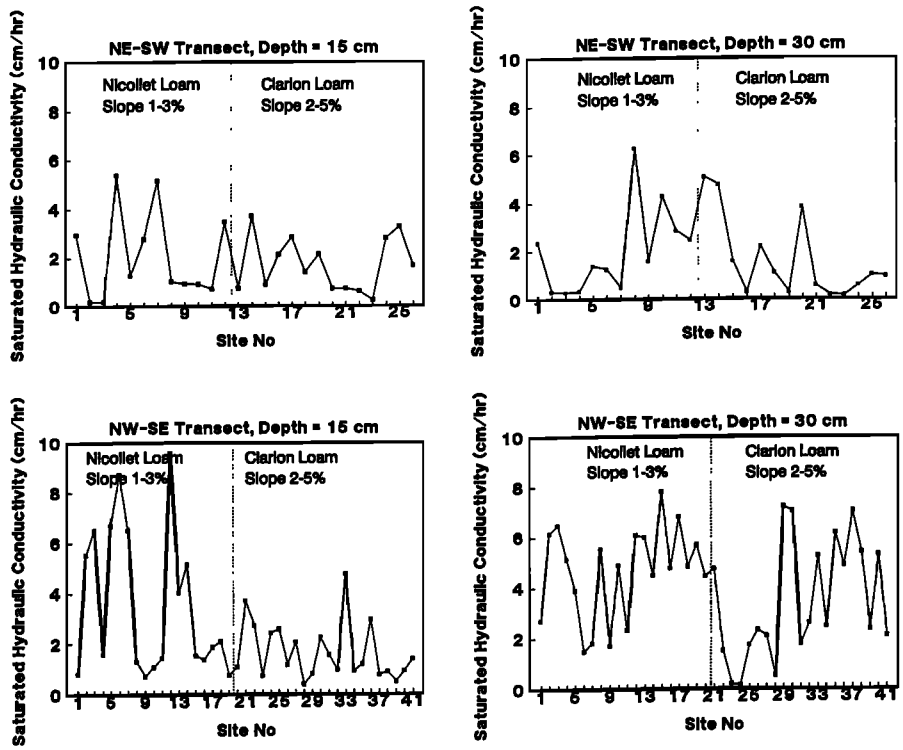

Figure 3. Saturated hydraulic conductivity along the NE-SW and NW-SE transects at 15-cm and 30-cm depths.

were different in size and density at different depths because of differential growth and density of plant roots and earthworm activities. Using automatic image analysis and AUTOCAD techniques, they showed that the total number of macropores was higher below the 30-cm depth than at the 15-cm depth in our no-till field.

All 134 soil water retention functions for both soil-slope combinations were evaluated qualitatively by eye. Although some variations existed, a typical trend in the $\theta(h)$ data was observed for each soil-slope type (Figure 4). The soil water content near saturation for the Nicollet loam soil was found to be higher than for the Clarion loam soil for several retention

Table 1. Summary Statistics of Measured Soil Hydraulic Parameters[a]

Parameter	Depth 15 cm		Depth 30 cm	
	Nicollet Loam With 1–3% Slope	Clarion Loam With 2–5% Slope	Nicollet Loam With 1–3% Slope	Clarion Loam With 2–5% Slope
		K_{sat}, cm h^{-1}		
Observations	82	103	87	101
Average	2.96[b]	1.61[c]	3.61[b]	2.84[b]
Standard deviation	2.58	1.09	2.21	2.25
Maximum	9.58	4.73	7.78	7.18
Minimum	0.19	0.22	0.27	0.11
		$\theta_{15,000}$, cm^3 cm^{-3}		
Observations	18	41	31	44
Average	0.109[b]	0.096[c]	0.119[b]	0.107[c]
Standard deviation	0.010	0.011	0.013	0.014
Maximum	0.137	0.124	0.177	0.150
Minimum	0.094	0.075	0.098	0.085
		$\theta_{333-15,000}$, cm^3 cm^{-3}		
Observations	12	25	7	26
Average	0.132[b]	0.119[b]	0.145[b]	0.133[b]
Standard deviation	0.022	0.019	0.020	0.029
Maximum	0.160	0.157	0.163	0.216
Minimum	0.091	0.083	0.102	0.094

[a]Multiple mean comparison for each depth was made using TUKEY statistics in SAS software.
[b]These values have no significant difference at 5% probability level.
[c]These values have no significant difference at 5% probability level.

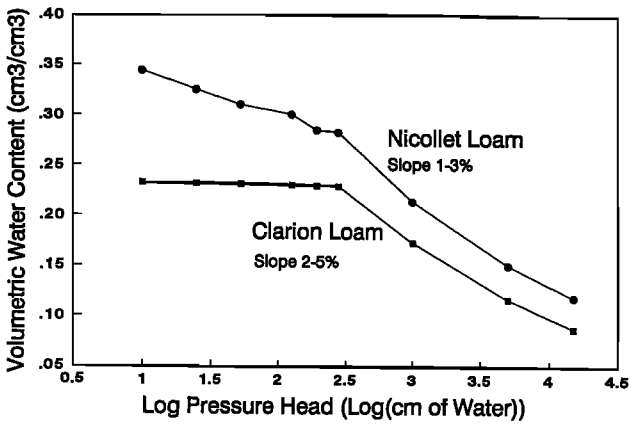

Figure 4. Typical soil water retention curves for the soil-slope combination at the field site. Nicollet loam (1–3%) data are for site 3 on the NE limb at 15-cm depth. Clarion loam (2–5%) data are for site 4 on the SW limb at 30-cm depth.

curves measured on the NE-SW transect at 30-cm depth. Two other hydrologic parameters (water content at the permanent wilting point $\theta_{15,000}$ and water-holding capacity, i.e., difference of water contents between the tensions of 333-cm and 15,000-cm H_2O, $\theta_{333-15,000}$) relevant to soil-vegetation-atmospheric interactions were investigated for possible correlation with the soil-slope combinations. More in-depth definitions and soil-related variations of these parameters are given by *Cassel and Nielsen* [1986]. The $\theta_{15,000}$ is expected to be related to the fine-textured particles (clay content) which varies with the slope positions. In Figure 4 the typical difference in $\theta_{15,000}$ is visible for Nicollet loam with 1–3% slope on the hilltop and Clarion loam with 2–5% slope on the shoulder position. However, $\theta_{333-15,000}$ is related to a wider distribution of particle sizes including silt and clay. The measured $\theta_{15,000}$ and $\theta_{333-15,000}$ values are plotted along both the NW-SE and NE-SW transects for the 15-cm and 30-cm depths (Figures 5 and 6). For two (laboratory water retention) measurement batches, water content is not available at a tension of ~333 cm, thus limiting the number of $\theta_{333-15,000}$ to 70 as compared to the sample size of 134 for $\theta_{15,000}$ and other soil water retention parameters. Mean comparison for $\theta_{333-15,000}$ showed no statistically significant difference (at 5% probability level) between depths or soil-slope combinations (Table 1). This finding is further corroborated by the observations of limited drift or trend across the soil-slope transition (as shown in Figure 6). On the contrary, $\theta_{15,000}$ showed statistically significant differences across the soil-slope transition for both the depths. A statistical comparison across depth indicated different behavior for Nicollet loam (on the hilltop) versus Clarion loam (on the slope). For Nicollet loam, $\theta_{15,000}$ are statistically similar for 15-cm and 30-cm depths; for Clarion loam, $\theta_{15,000}$ are statistically different for the two depths. These findings are extremely critical for understanding the soil moisture dynamics and related hydrologic processes of evapotranspiration, infiltration, and runoff at larger (spatial) scales with complex terrain (e.g., rolling topography, hill-slope, catchment, and watershed) and geohydrological settings. Moreover, they provide useful guidance for sampling design under a complex terrain in other hydrologic studies (e.g., SGP97 Hydrology Experiment [*Mohanty et al.*, 2000]).

The *van Genuchten* [1980] soil water retention parameters were estimated using the RETC optimization algorithm. Among 134 model runs for different soil cores, 118 data sets converged with modeled-to-observed R^2 greater than 0.98. The other 16 sets were discarded when the modeled-to-observed R^2 fell below 0.98 (M. T. van Genuchten, personal communication, 1999). The correlation matrix for the reten-

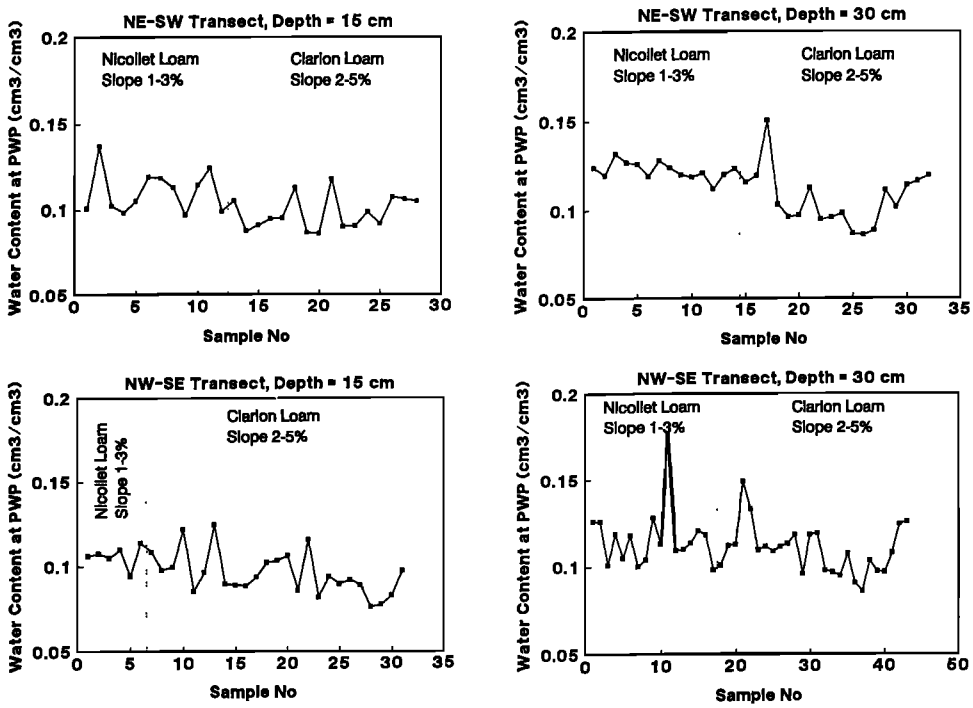

Figure 5. Water content at permanent wilting point $\theta_{15,000}$ (PWP) along the NE-SW and NW-SE transects at 15-cm and 30-cm depths. Replicates are juxtaposed for plotting.

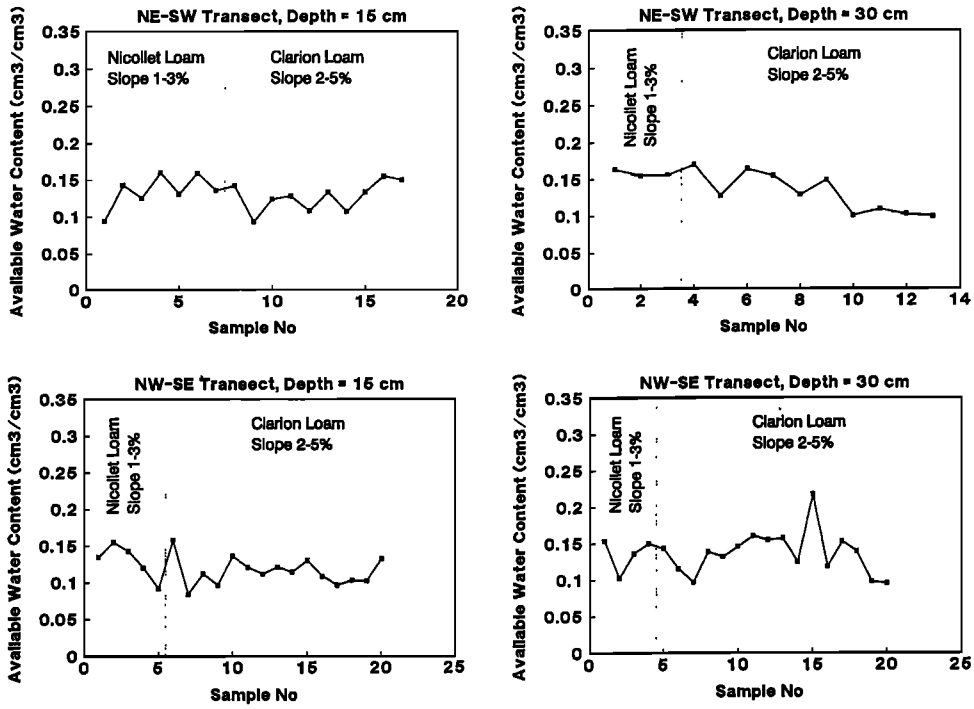

Figure 6. Available water content $\theta_{333-15,000}$ along the NE-SW and NW-SE transects at 15-cm and 30-cm depths. Replicates are juxtaposed for plotting.

tion parameters is reported in Table 2. For all cases the correlation coefficient between the fitted parameters was lower than the suggested limit (0.90 (M. T. van Genuchten, personal communication, 1999)), indicating no further analysis is necessary with (any) fixed parameter(s). The optimized θ_s, θ_r, α, and n values are plotted along both the NW-SE and NE-SW transects for the 15-cm and 30-cm depths (Figures 7, 8, and 9). Interestingly, for all four optimized hydraulic parameters (θ_s, θ_r, α, and n) no significant trend across the two soil-slope combinations was observed except in a few occasions: θ_s at the 30-cm depth on the NE-SW transect and α at the 30-cm depth on the NW-SE transect. Classical statistics for these parameters with mean comparison between the soil-slope combinations are given in Table 3. At the 15 cm depth for θ_s, α, and n, statistically significant differences (at 5% probability level) were observed between the Nicollet loam on the hilltop and Clarion loam on the shoulder positions. Furthermore, at the 30-cm depth, statistically significant differences were found only for θ_s and θ_r across the soil-slope transition. Comparison of soil water retention parameters between the two depths showed statistically significant differences for θ_s, θ_r, and α but not for n. All these findings suggest that the pore size distribution varies with the soil-slope combination and depth. Also, note that the (measured) $\theta_{15,000}$ and the (optimized) θ_r, which at times are assumed to be the same in the soil hydrology, showed distinctly different spatial characteristics.

Table 2. Correlation Matrix of Soil Water Retention Parameters for RETC Runs[a]

	θ_r	θ_s	α	n
		Depth 15 cm		
θ_r	1			
θ_s	0.0138	1		
α	0.330	0.049	1	
n	0.776	0.0008	0.320	1
		Depth 30 cm		
θ_r	1			
θ_s	0.0008	1		
α	0.370	0.083	1	
n	0.675	0.0238	0.373	1

[a]RETC is an optimization computer code. Data are pooled for both the soil-slope combinations for this analysis.

The measured (K_{sat}, $\theta_{15,000}$, and $\theta_{333-15,000}$) and optimized (θ_s, θ_r, α, and n) hydraulic parameters were tested for normality using exploratory data analysis techniques (e.g., stem-and-leaf plot and normal probability plot) and the Shapiro-Wilk test (SAS Institute, Inc., Cary, North Carolina). For most of the parameters (K_{sat}, $\theta_{15,000}$, $\theta_{333-15,000}$, α, and n), normality was better achieved by $\log_e$ transformation than the raw data, except in few occasions. Only for θ_s and θ_r, was normality better for the raw data than the $\log_e$-transformed data. Table 4 summarizes the W statistics for all raw and $\log_e$-transformed data. For the sake of brevity, sample stem-and-leaf plots and normal probability plots of the raw and $\log_e$-transformed data for (more lognormal) α at 15-cm depth are presented in Figure 10. $\log_e$ transformation squeeze or spread the data set to obtain a more bell-shaped Gaussian curve and yield good results in transforming the nonnormal data sets to nearly normal data sets. All K_{sat}, $\theta_{15,000}$, $\theta_{333-15,000}$, α, and n data were therefore log transformed and these $\log_e$ ( ) values were used for further analysis. Subsequently, any deterministic drift across the soil-slope transition was removed from the normal(ized) data set using the mean-polishing approach (equation (4)) leaving behind more stationary residuals ($\varepsilon(x)$) for structural analysis. The mean polishing of $\log_e$-transformed data also concurs with the additive rules of *Cressie* [1985] that are nec-

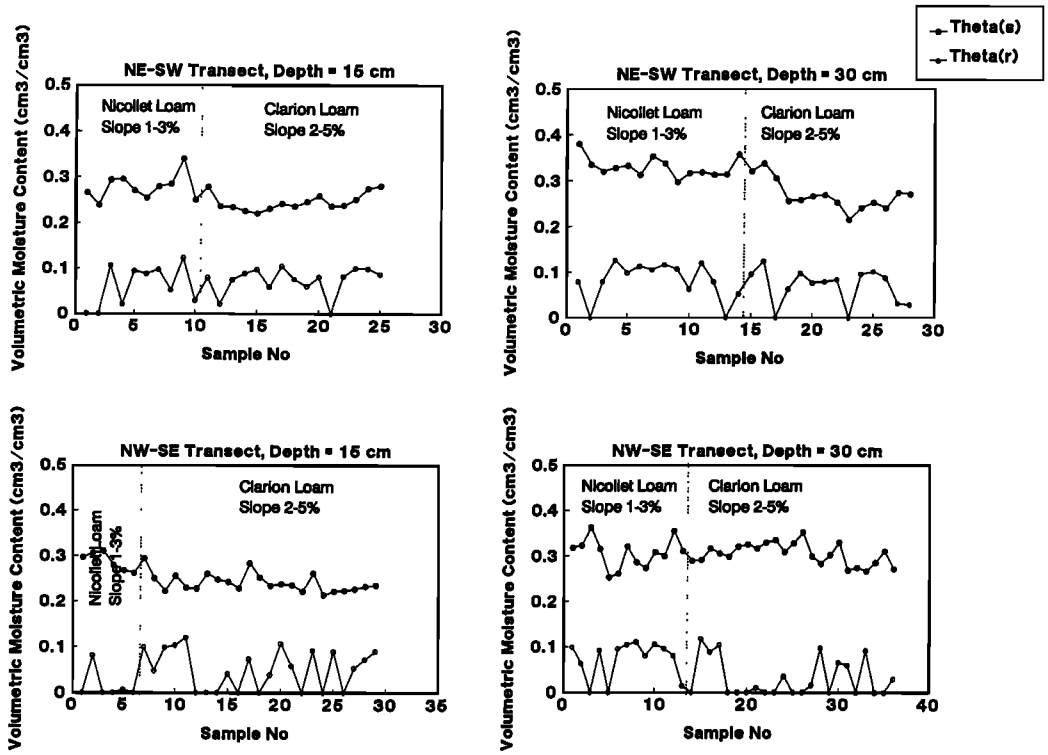

Figure 7. Saturated water content θ_s and residual water content θ_r, along the NW-SE and NE-SW transects at 15-cm and 30-cm depths. Replicates are juxtaposed for plotting.

essary for spatial analysis. Further discussion on related issues is given by *Cressie* [1993] and *Mohanty et al.* [1991].

3.2. Structural Analysis

Experimental semivariograms (equation (3)) were developed for $\log_e K_{sat}$, $\log_e \theta_{15,000}$, $\log_e \theta_{333-15,000}$, θ_s, θ_r, $\log_e \alpha$, and $\log_e n$ using the stationary and normalized residuals across the entire field. Isotropic two-dimensional experimental semivariograms were calculated up to the maximum lag (~180 m). As the number of pairs reduced below 30 (a standard geostatistical rule) at the larger lags, we limited the active lag to 90 m for model fitting and analysis purposes. Assuming no nested spatial structure, different models (equations (6)–(9)) were fitted to the experimental semivariograms in turn. For the

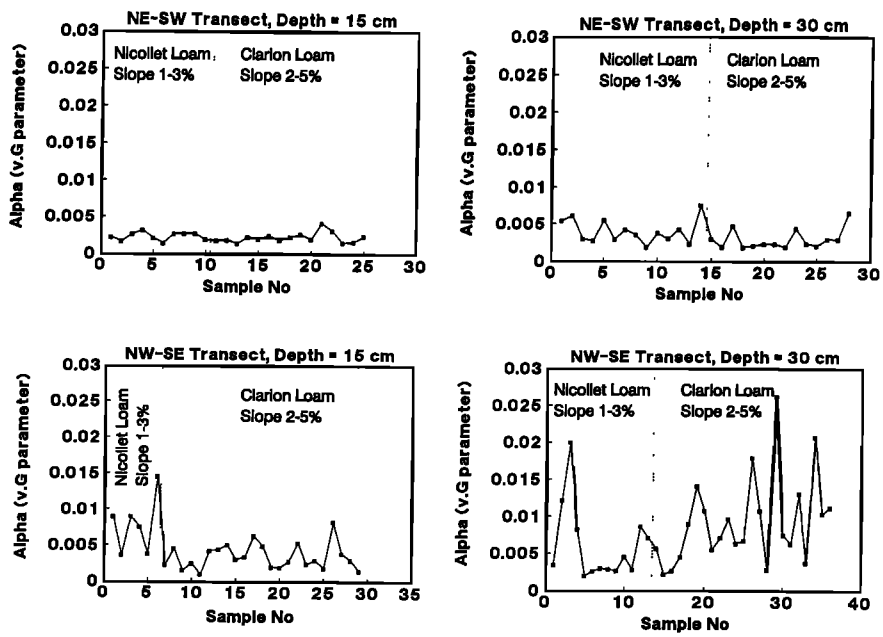

Figure 8. The van Genuchten parameter (α) along the NE-SW and NW-SE transects at 15-cm and 30-cm depths. Replicates are juxtaposed for plotting.

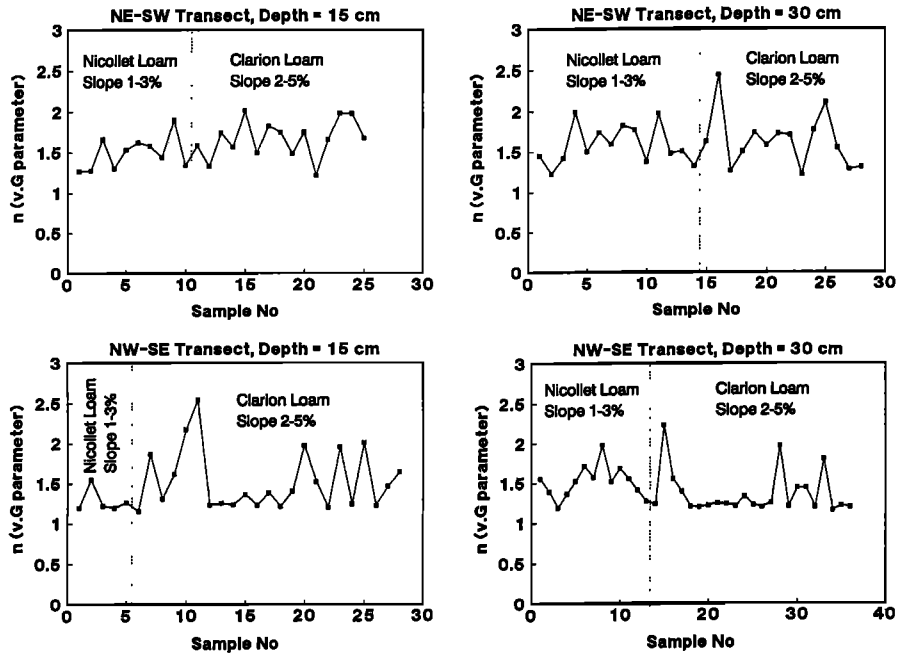

Figure 9. The van Genuchten parameter (n) along the NE-SW and NW-SE transects at 15 cm and 30 cm depths. Replicates are juxtaposed for plotting.

best fit model(s), structural variance (C), nugget variance including subgrid variability (C_0), range or range parameter (A_0), reduced sum of squares (RSS), and coefficient of determination (r^2) are listed in Table 5. Experimental semivariograms with the fitted theoretical model are shown in Figure 11. Besides the isotropic two-dimensional experimental semivariograms, we also calculated the directional semivariograms in four directions (θ = 0°, 45°, 90°, and 135°) with 0° matching to

Table 3. Summary Statistics of Optimized Soil Water Retention Parameters[a]

Parameter	Depth 15 cm		Depth 30 cm	
	Nicollet Loam With 1–3% Slope	Clarion Loam With 2–5% Slope	Nicollet Loam With 1–3% Slope	Clarion Loam With 2–5% Slope
		θ_s, $cm^3\ cm^{-3}$		
Observations	16	38	27	37
Average	0.281[b]	0.243[c]	0.318[b]	0.291[c]
Standard deviation	0.025	0.019	0.0290	0.0315
Maximum	0.340	0.295	0.381	0.352
Minimum	0.239	0.215	0.252	0.216
		θ_r, $cm^3\ cm^{-3}$		
Observations	16	38	27	37
Average	0.0436[b]	0.0605[b]	0.076[b]	0.0450[c]
Standard deviation	0.045	0.0394	0.0395	0.0437
Maximum	0.123	0.120	0.126	0.125
Minimum	0.0	0.0	0.0	0.0
		α, cm^{-1}		
Observations	16	38	27	37
Average	0.0043[b]	0.0029[c]	0.0050[b]	0.0069[b]
Standard deviation	0.0035	0.0015	0.0037	0.0055
Maximum	0.0145	0.0083	0.0199	0.0259
Minimum	0.0013	0.0010	0.0018	0.0018
		n (dimensionless)		
Observations	16	38	27	37
Average	1.408[c]	1.60[b]	1.55[b]	1.46[b]
Standard deviation	0.207	0.320	0.216	0.318
Maximum	1.90	2.54	1.99	2.43
Minimum	1.15	1.19	1.19	1.15

[a]Multiple mean comparison for each depth was made using TUKEY statistics in SAS software.
[b]These values have no significant difference at 5% probability level.
[c]These values have no significant difference at 5% probability level.

Table 4. Shapiro-Wilk W Statistics for Raw and Log_e-Transformed Soil Hydraulic Parameters[a]

	Depth 15 cm[b]		Depth 30 cm[b]	
Parameter	Raw	Log_e	Raw	Log_e
K_{sat}	0.795 (<0.0001)	0.975 (0.2284)	0.923 (0.0007)	0.869 (<0.0001)
$\theta_{15,000}$	0.979 (0.409)	0.991 (0.9447)	0.929 (0.0004)	0.963 (0.0312)
$\theta_{333-15,000}$	0.968 (0.361)	0.964 (0.2647)	0.929 (0.0324)	0.930 (0.0369)
θ_s	0.929 (0.0035)	0.948 (0.0214)	0.982 (0.5226)	0.971 (0.1414)
θ_r	0.865 (<0.0001)	0.826 (<0.0001)	0.853 (<0.0001)	0.828 (<0.0001)
α	0.727 (<0.0001)	0.951 (0.0294)	0.773 (<0.0001)	0.944 (0.0061)
n	0.914 (0.0009)	0.937 (0.0073)	0.901 (<0.0001)	0.932 (0.0017)

[a] W statistics were calculated using SAS Institute, Inc. (Cary, North Carolina) software.
[b] Numbers inside parentheses indicate probability level.

the SE limb of the orthogonal transects. Anisotropic theoretical models as defined in (6)–(10) were used, and the optimized parameters are shown in Figure 12 along with a sample fit. During the fitting of theoretical models for isotropic (Table 5) and anisotropic (Table 6) semivariograms, in few instances, we have listed more than one model to minimize any judgmental error of one model over the other with minor gain in r^2 and/or reduction in RSS. Although somewhat redundant, this information may prove to be useful for designing more efficient sampling schemes for future hydrologic experiments. For example, similar fits with exponential and spherical models will have different correlation ranges and therefore may lend different sampling designs. In sections 3.2.1–3.2.7 we will discuss the spatial structures and suggest possible physical processes/factors contributing to the spatial variability of individual parameters at the 15-cm and 30-cm depths.

3.2.1. Saturated hydraulic conductivity (K_{sat}). Structural analyses of $\log_e K_{sat}$, shown in Figures 11a and 11b and 12a and 12b, indicate better spatial structure at the 30-cm depth than at the 15-cm depth. Considering a spherical model to adequately describe the isotropic semivariogram, a correlation range of 60.5 m was discovered for the 30-cm depth. On the

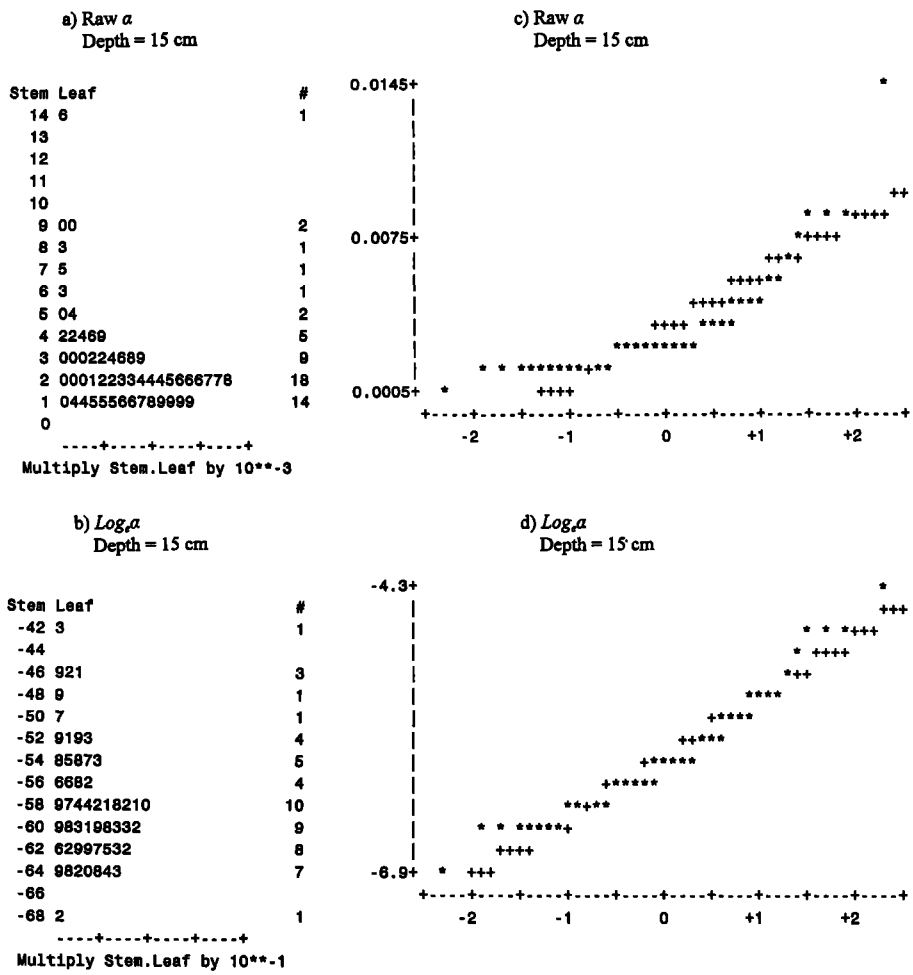

Figure 10. Stem-and-leaf plot for (a) raw α and (b) $\log_e \alpha$ and normal probability plot for (c) raw α and (d) $\log_e \alpha$ at 15-cm depth.

Table 5. Isotropic Models of Different Hydraulic Parameters[a]

Parameter	Model Type	C_0	$C_0 + C$	A_0, m	RSS	r^2
	Depth 15 cm					
$\text{Log}_e K_{sat}$($\log_e$, cm h^{-1})	linear	0.52	>0.96	>90.0	0.232	0.522
	spherical	0.52	1.03	144.8	0.240	0.506
	Gaussian	0.57	1.12	134.2	0.203	0.583
$\text{Log}_e \theta_{333-15,000}$($\log_e$, cm^3 cm^{-3})	spherical	0.0033	0.0323	13.3	0.0008	0.383
$\text{Log}_e \theta_{15,000}$($\log_e$, cm^3 cm^{-3})	linear	0.0125	>0.0126	>90.0	5×10^{-5}	0.000
θ_s, cm^3 cm^{-3}	spherical	0.0002	0.00048	20.3	2×10^{-7}	0.273
θ_r, cm^3 cm^{-3}	spherical	0.0015	0.00186	67.2	1×10^{-6}	0.178
$\text{Log}_e \alpha$($\log_e$, cm^{-1})	linear	0.19	>0.34	>90.0	0.0237	0.605
	spherical	0.18	0.33	99.9	0.0237	0.603
	Gaussian	0.19	0.32	78.5	0.0230	0.616
$\text{Log}_e n$, dimensionless	linear	0.0352	>0.0352	>90.0	0.0012	0.034
	Depth 30 cm					
$\text{Log}_e K_{sat}$($\log_e$, cm h^{-1})	spherical	0.55	1.59	60.5	0.2773	0.854
	exponential	0.49	1.73	30.2	0.3781	0.802
	Gaussian	0.72	1.61	54.8	0.2925	0.846
$\text{Log}_e \theta_{333-15,000}$($\log_e$, cm^3 cm^{-3})	exponential	0.02	0.048	26.4	0.0033	0.230
$\text{Log}_e \theta_{15,000}$($\log_e$, cm^3 cm^{-3})	spherical	0.007	0.0153	15.7	0.0002	0.178
θ_s, cm^3 cm^{-3}	spherical	0.00023	0.0011	57.0	1×10^{-6}	0.588
	exponential	0.00016	0.0012	24.2	1×10^{-6}	0.523
	Gaussian	0.00035	0.0011	48.9	1×10^{-6}	0.576
θ_r, cm^3 cm^{-3}	exponential	0.0007	0.0019	4.2	3×10^{-6}	0.160
$\text{Log}_e \alpha$($\log_e$, cm^{-1})	spherical	0.142	0.461	42.2	0.2389	0.401
	Gaussian	0.188	0.464	37.6	0.2410	0.396
$\text{Log}_e n$, dimensionless	spherical	0.017	0.032	16.5	0.0007	0.187

[a]Definitions are as follows: C_0, nugget variance including subgrid variability; C, structural variance; A_0, range or range parameter; RSS, reduced sum of squares; and r^2, coefficient of determination.

contrary, relatively higher nugget variance and smaller structural variance were observed at the 15-cm depth. We suggest that higher disturbances due to agricultural (traffic, tillage, differential root, and worm activities) and hydrologic (precipitation and freezing-thawing) activities at the 15-cm as compared to 30-cm depth contributed to the difference in spatial structures. Anisotropic behavior was observed for both depths with a more pronounced effect at the 30-cm depth. The higher anisotropy at 30-cm depth is related to the underlying depositional process of glacial till, features that have been smeared by environmental influences at the shallower depth. A more in-depth discussion of the spatial and depth variability of K_{sat} including different measurement techniques is given by *Mohanty et al.* [1991, 1994].

3.2.2. Water-holding capacity ($\theta_{333-15,000}$). Water-holding capacity is popularly used in many bucket-type (i.e., water balance) soil hydrologic models. Distinct differences in the spatial structure of $\log_e \theta_{333-15,000}$ were observed with significant random noise for the two depths (Figures 11c and 11d and 12c and 12d). Some amount of spherical or cyclic

Table 6. Anisotropic Models of Different Hydraulic Parameters

Parameter	Model Type	C_0	$C_0 + C$	A_1, m	A_2, m	RSS	r^2
	Depth 15 cm						
$\text{Log}_e K_{sat}$($\log_e$, cm h^{-1})	linear	0.31	0.96	44.3	82.3	6.97	0.405
	spherical	0.24	1.22	59.3	154.8	6.97	0.373
	Gaussian	0.38	1.31	60.2	143.1	6.50	0.410
$\text{Log}_e \theta_{333-15,000}$($\log_e$, cm^3 cm^{-3})	spherical	0.0001	0.036	3.9	14.2	0.041	0.187
$\text{Log}_e \theta_{15,000}$($\log_e$, cm^3 cm^{-3})	linear	0.0125	0.0126	45.2	45.2	0.001	0.012
θ_s, cm^3 cm^{-3}	linear	0.00045	0.00047	5.3	915	0.0	0.060
θ_r, cm^3 cm^{-3}	spherical	0.0012	0.0019	81.8	81.8	0.0	0.267
$\text{Log}_e \alpha$($\log_e$, cm^{-1})	linear	0.22	0.30	74.7	74.7	1.73	0.089
$\text{Log}_e n$, dimensionless	exponential	0.0314	0.0337	8.0	8.0	0.019	0.227
	Depth 30 cm						
$\text{Log}_e K_{sat}$($\log_e$, cm h^{-1})	spherical	0.50	2.12	45.5	116	26.05	0.476
	exponential	0.13	2.04	12.9	33.9	28.57	0.445
	Gaussian	0.75	2.14	40.3	102.8	26.31	0.461
$\text{Log}_e \theta_{333-15,000}$($\log_e$, cm^3 cm^{-3})	linear	0.021	0.053	53.4	78.9	0.0669	0.180
$\text{Log}_e \theta_{15,000}$($\log_e$, cm^3 cm^{-3})	exponential	0.0042	0.0143	3.6	3.6	0.0035	0.054
θ_s, cm^3 cm^{-3}	spherical	0.00017	0.0011	39.9	80.6	0.0	0.329
	exponential	0.00010	0.0012	15.8	36.2	0.0	0.294
	Gaussian	0.00034	0.0012	34.4	75.7	0.0	0.324
θ_r, cm^3 cm^{-3}	linear	0.002	0.0018	40.4	63.5	0.0	0.071
$\text{Log}_e \alpha$($\log_e$, cm^{-1})	spherical	0.10	0.45	41.8	41.8	4.11	0.213
$\text{Log}_e n$, dimensionless	linear	0.041	0.031	43.9	52.2	0.011	0.171

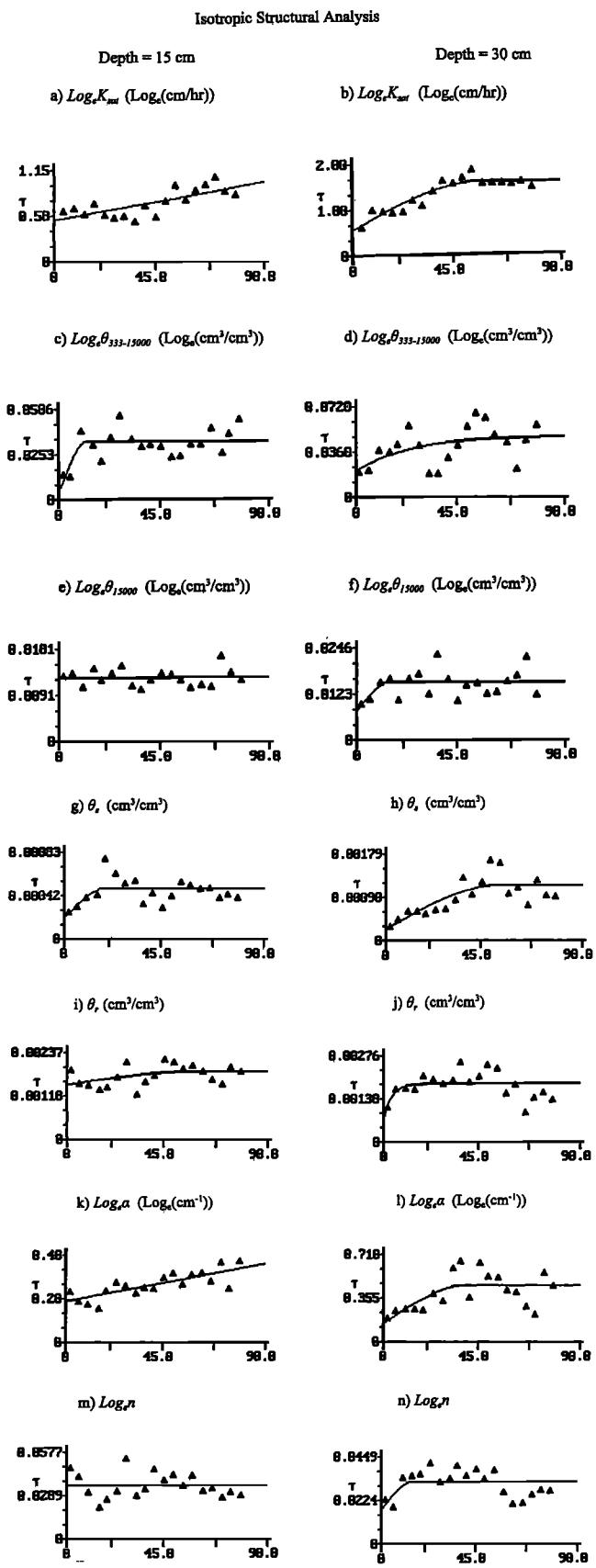

Figure 11. Isotropic experimental semivariogram with fitted theoretical model for different hydraulic parameters at (a), (c), (e), (g), (i), (k), and (m) 15-cm and (b), (d), (f), (h), (j), (l), and (n) 30-cm depths. X axis indicates lag distance in meters.

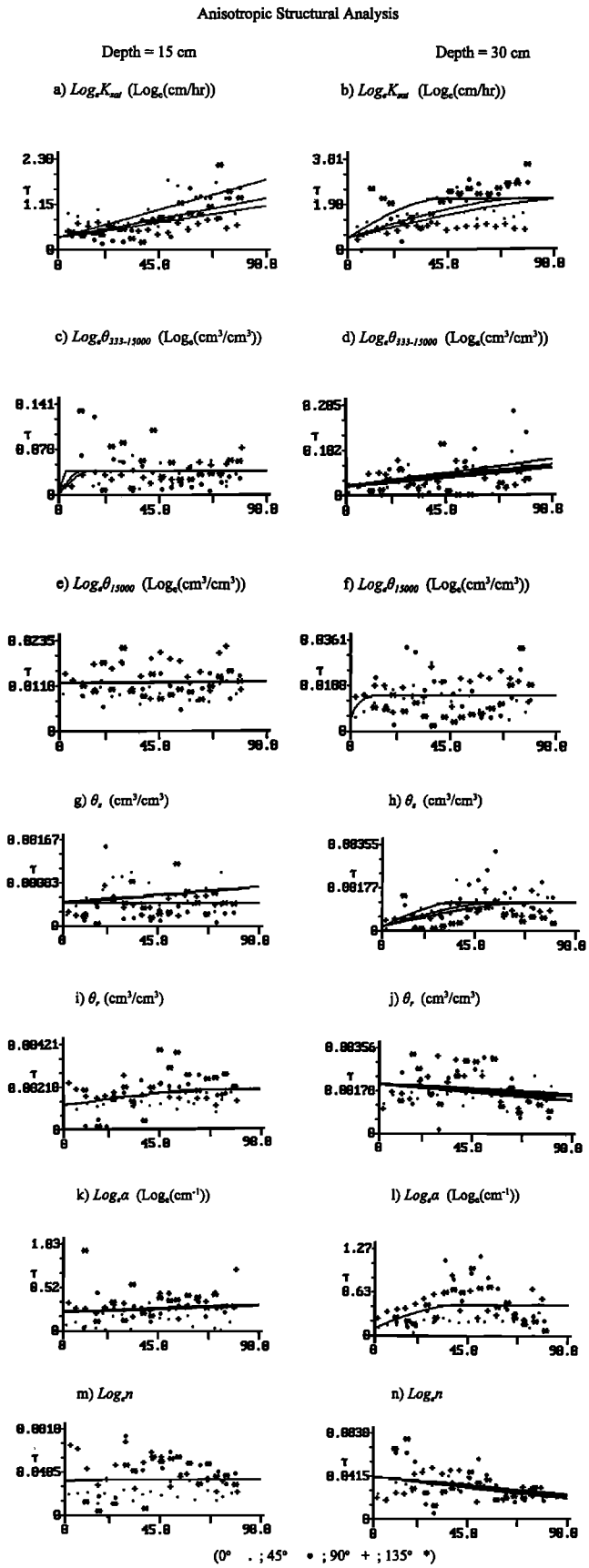

Figure 12. Anisotropic experimental semivariogram with fitted theoretical model for different hydraulic parameters at (a), (c), (e), (g), (i), (k), and (m) 15-cm and (b), (d), (f), (h), (j), (l), and (n) 30-cm depths. X axis indicates lag distance in meters. Four angles (φ = 0°, 45°, 90°, and 135°) between pairs were considered with angle of maximum variation (Φ) equal to 0°.

pattern is visible in the experimental semivariograms which may be an artifact (with low r^2) because of the limited sample size and data gaps for $\theta_{333-15,000}$ (as described in section 3.1). Also note that $\theta_{333-15,000}$ is the only parameter for which we did not find any deterministic drift related to soil-slope combinations during the preprocessing of data.

3.2.3. Water content at permanent wilting point ($\theta_{15,000}$). No spatial structure could be identified for $\log_e \theta_{15,000}$ for either of the two depths (Figures 11e and 11f and 12e and 12f). Microheterogeneity and subgrid-scale variability dominated the spatial structure with some amount of directional anisotropy. It is consistent with the physical basis of the $\theta_{15,000}$ parameter which is related to the uniform texture of the soil at the field site.

3.2.4. Saturated water content (θ_s). Interestingly, spatial variability for independently optimized θ_s (Figures 11g and 11h and 12g and 12h) matched closely with the spatial structure of measured K_{sat} (Figures 11a and 11b and 12a and 12b) for both the depths. This finding is somewhat expected based on the traditional definition of the relationship between soil water retention and hydraulic conductivity assuming the unimodal pore size distribution of the van Genuchten-Mualem relationship [*van Genuchten*, 1980]. More recent studies show evidence of macroporosity in the field soils and limited relationship between the two (K_{sat} and θ_s) parameters [*Mohanty et al.*, 1997]. While macropores were observed in this no-tillage field [*Singh et al.*, 1991], their effect has been smeared out by using average K_{sat} (for three replicates) at each grid location.

3.2.5. Residual water content (θ_r). As for measured $\theta_{15,000}$, the optimized residual water content (θ_r) showed limited spatial structure for both depths (Figures 11i and 11j and 12i and 12j). The limited structure demonstrates the dominance of microheterogeneity in this texture-related soil hydraulic parameter at the field site. In addition, being a fitting parameter with limited data at the lower pressure range, θ_r was more prone to uncertainties [*van Genuchten*, 1980].

3.2.6. The van Genuchten parameter (α). The soil water retention parameter ($\log_e \alpha$), inverse of the bubbling pressure, was found to have reasonably good spatial correlation structure for both 15-cm and 30-cm depths (Figures 11k and 11l and 12k and 12l). Consistent with $\log_e K_{sat}$ and θ_s, a relatively higher nugget effect ($C_0/C + C_0$) was observed for $\log_e \alpha$ at 15-cm depth in comparison with 30-cm depth. The correlation length (A_0) was 60 m (or more) for 15-cm depth and 15 m (or more) for 30-cm depth with little apparent directional anisotropy. From a physical perspective, α in the van Genuchten soil water retention function relates to the mean pore size (or a scale factor describing the linear component), whereas n (described in section 3.2.7) relates to the spread of the pore size distribution (or a shape factor describing the nonlinear component) [*Vogel et al.*, 1991; M. G. Schaap, personal communication, 2000]. Being dominated by the magnitude/scale of the pore size distribution, α behaves more like other (macro and micro) porosity-related parameters (K_{sat} and θ_s).

3.2.7. The van Genuchten parameter (n). The shape parameter ($\log_e n$) of the van Genuchten-Mualem relationship showed limited spatial structure for either depth (Figures 11m and 11n and 12m and 12n). This is because n is related to the spread of the pore or particle size distribution (i.e., soil texture) which is more or less uniform (loam) across the field.

By grouping the results for the hydraulic parameters into two broad categories, we suggest that the (macro and micro) porosity-related parameters ($\log_e K_{sat}$, θ_s, and $\log_e \alpha$) are spatially related with relatively large correlation lengths, whereas the texture-related parameters ($\log_e \theta_{333-15,000}$, $\log_e \theta_{15,000}$, θ_r, and $\log_e n$) are dominated by microheterogeneity and subgrid-scale variability at the field site. These intriguing new findings may help with designing and evaluating the effectiveness of process-based hydrologic models using van Genuchten-Mulaem hydraulic relationships versus simplistic water balance models at field scales or larger scales.

4. Summary and Conclusions

Hydraulic properties were measured on two orthogonal transects at two depths cutting across a soil-slope transition (Nicollet loam with 1–3% slope on the hilltop and Clarion loam with 2–5% slope on the shoulder position) in a glacial till soil in Iowa. Exploratory and geostatistical data analyses were performed to study the spatial variability of the measured (K_{sat}, $\theta_{15,000}$, and $\theta_{333-15,000}$) or optimized (θ_s, θ_r, α, and n) hydraulic parameters. Results indicated that most of these parameters are significantly different across the soil-slope transition except $\theta_{333-15,000}$. Furthermore, the (macro and micro) porosity-related parameters ($\log_e K_{sat}$, θ_s, and $\log_e \alpha$) are spatially related with relatively large correlation lengths, whereas the texture-related parameters ($\log_e \theta_{333-15,000}$, $\log_e \theta_{15,000}$, θ_r, and $\log_e n$) are dominated by microheterogeneity and subgrid-scale variability at the field site. A higher nugget effect at the 15-cm depth in comparison with the 30-cm depth indicates surface disturbances due to agricultural activities. We suggest that a uniform texture (loam) and a pore size distribution developed by long-term (no tillage) agricultural practices in the field are important controlling factors for the spatial variability of different hydraulic parameters. However, further research is necessary to study whether the control for all hydraulic properties (including soil water retention $\theta(h)$ and unsaturated hydraulic conductivity $K(h)$) changes at different spatial scales depending on the complexity of terrain, including different soil-slope-vegetation management combinations at a hierarchy of spatial scales. The current results and future findings will be useful for large-scale (e.g., field, basin, watershed, and region) soil moisture variability, land surface hydrologic, and contaminant transport studies.

Acknowledgments. Field and laboratory experiments were conducted at Iowa State University, Ames, Iowa. Data analysis effort was partially supported by the NASA—Land Surface Hydrology (LSH) program through grant NAG5-8682.

References

Azevedo, A. S., R. S. Kanwar, and R. Horton, Effect of cultivation on hydraulic properties of an Iowa soil using tension infiltrometer, *Soil Sci., 163*, 22–29, 1998.

Cassel, D. K., and D. R. Nielsen, Field capacity and available water capacity, in *Methods of Soil Analysis, Part 1: Physical and Mineralogical Methods*, vol. 9, 2nd ed., edited by A. Klute, pp. 901–926, Am. Soc. of Agron., Madison, Wis., 1986.

Cressie, N. A. C., When are relative variograms useful in geostatistics? *J. Math. Geol., 17*, 693–702, 1985.

Cressie, N. A. C., *Statistics for Spatial Data*, 900 pp., John Wiley, New York, 1993.

Elsenbeer, H., K. Cassel, and J. Castro, Spatial analysis of soil hydraulic conductivity in a tropical rain forest catchment, *Water Resour. Res., 28*, 3201–3214, 1992.

Famiglietti, J. S., J. W. Rudnicki, and M. Rodell, Variability in surface soil moisture content along a hillslope transect: Rattlesnake hill, Texas, *J. Hydrol., 210*, 259–281, 1998.

Gajem, Y. M., A. W. Warrick, and D. E. Myers, Spatial dependence of physical properties of typic Torrifluvent soil, *Soil Sci. Soc. Am. J.*, *45*, 709–715, 1981.

Hussain, I., K. R. Olson, and J. C. Siemens, Long-term effects on physical properties of eroded soil, *Soil Sci.*, *163*, 970–981, 1998.

Journel, A., and C. J. Huijbregts, *Mining Geostatistics*, 600 pp., Academic, San Diego, Calif., 1978.

Klute, A. (Ed.), *Methods of Soil Analysis, Part 1: Physical and Mineralogical Methods*, vol. 9, 2nd ed., 1188 pp., Am. Soc. Agron., Madison, Wis., 1986.

Loague, K., and G. A. Gander, R-5 revisited, 1, Spatial variability of infiltration on a small rangeland catchment, *Water Resour. Res.*, *26*, 957–971, 1990.

Logsdon, S. D., and D. B. Jaynes, Spatial variability of hydraulic conductivity in a cultivated field at different times, *Soil Sci. Soc. Am. J.*, *60*, 703–709, 1996.

Mallants, D., B. P. Mohanty, D. Jacques, and J. Feyen, Spatial variability of hydraulic properties in a multi-layered soil profile, *Soil Sci.*, *161*, 167–181, 1996.

Marquardt, D. W., An algorithm for least-squares estimation of nonlinear parameters, *J. Soc. Ind. Appl. Math.*, *11*, 431–441, 1963.

Matheron, G., Principles of geostatistics, *Econ. Geol.*, *58*, 1246–1266, 1963.

Mohanty, B. P., and R. S. Kanwar, Spatial variability of residual nitrate-nitrogen under two tillage systems in central Iowa: A composite three-dimensional resistant and exploratory approach, *Water Resour. Res.*, *30*, 237–251, 1994.

Mohanty, B. P., R. S. Kanwar, and R. Horton. A robust-resistant approach to interpret spatial behavior of saturated hydraulic conductivity of a glacial till soil under no-tillage system, *Water Resour. Res.*, *27*, 2979–2992, 1991.

Mohanty, B. P., M. D. Ankeny, R. Horton, and R. S. Kanwar, Spatial analysis of hydraulic conductivity measured using disc infiltrometers, *Water Resour. Res.*, *30*, 2489–2498, 1994.

Mohanty, B. P., R. S. Bowman, J. M. H. Hendrickx, and M. T. van Genuchten, New piecewise-continuous hydraulic functions for modeling preferential flow in an intermittent-flood-irrigated field, *Water Resour. Res.*, *33*, 2049–2063, 1997.

Mohanty, B. P., T. H. Skaggs, and M. T. van Genuchten, Impact of saturated hydraulic conductivity on the prediction of tile flow, *Soil Sci. Soc. Am. J.*, *62*, 1522–1529, 1998.

Mohanty, B. P., T. H. Skaggs, and J. S. Famiglietti, Analysis and mapping of field-scale soil moisture variability using high-resolution ground-based data during the Southern Great Plains 1997 (SGP97) Hydrology Experiment, *Water Resour. Res.*, *36*(4), 1023–1031, 2000.

Russo, D., and E. Bresler, Soil hydraulic properties as a stochastic processes, I, An analysis of field spatial variability, *Soil Sci. Soc. Am. J.*, *45*, 682–687, 1981.

Sauer, T. J., P. A. Moore Jr., K. P. Coffey, and E. M. Rutledge, Characterizing the surface properties of soils at varying landscape positions in the Ozark highlands, *Soil Sci.*, *163*, 907–915, 1998.

Sharma, M. L., G. A. Gander, and C. C. Hunt, Spatial variability of infiltration in a watershed, *J. Hydrol.*, *45*, 101–122, 1980.

Singh, P., R. S. Kanwar, and M. L. Thompson, Measurement and characterization of macropores using AUTOCAD and automatic image analysis, *J. Environ. Qual.*, *20*, 289–294, 1991.

Tukey, J. W., *Exploratory Data Analysis*, Addison-Wesley-Longman, Reading, Mass., 1977.

Unlu, K., D. R. Nielsen, J. W. Biggar, and F. Morkoc, Statistical parameters characterizing the spatial variability of selected hydraulic properties, *Soil Sci. Soc. Am. J.*, *54*, 1537–1547, 1990.

U.S. Department of Agriculture, Soil survey of Boone County, report, Iowa Agric. and Home Econ. Exp. Stn., Ames, 1984.

van Genuchten, M. T., A closed-form equation for predicting the hydraulic conductivity of unsaturated soils, *Soil Sci. Soc. Am. J.*, *44*, 892–898, 1980.

van Genuchten, M. T., F. J. Leij, and S. R. Yates, The RETC code for quantifying the hydraulic functions of unsaturated soils, *U.S. EPA Rep. 600/2-91/065*, 85 pp., Environ. Protect. Agency, Washington, D. C., 1991.

Vogel, T., M. Cislerova, and J. W. Hopmans, Porous media with linearly variable hydraulic properties, *Water Resour. Res.*, *27*, 2735–2741, 1991.

Yates, S. R., M. T. van Genuchten, A. W. Warrick, and F. J. Leij, Analysis of measured, predicted, and estimated hydraulic conductivity using the RETC computer program, *Soil Sci. Soc. Am. J.*, *56*, 347–354, 1992.

B. P. Mohanty, U.S. Salinity Laboratory, 450 W. Big Springs Road, Riverside, CA 92507. (bmohanty@ussl.ars.usda.gov)

Z. Mousli, University of California Bay Area Research and Extension Center, 90 W. Winchester Boulevard, Santa Clara, CA 95050.

(Received April 27, 2000; revised July 10, 2000;
accepted July 17, 2000.)